# Numerical simulation of welding positions in Gas Tungsten Arc Welding

M. C. Nguyen, O. Asserin, S. Gounand, P. Gilles, M. Médale

# NUMERICAL SIMULATION OF WELDING POSITIONS IN GAS TUNGSTEN ARC WELDING

M. C. NGUYEN* ****, O. ASSERIN*, S. GOUNAND**,
P. GILLES***, M. MEDALE*****

*Atomic Energy Commission (CEA Saclay), DEN, DANS, DM2S, SEMT, LTA, F-91191, Gif-sur-Yvette, France
**Atomic Energy Commission (CEA Saclay), DEN, DANS, DM2S, STMF, LMSF, F-91191, Gif-sur-Yvette, France
***AREVA NP, F-92084, Paris La Défense, France
**** Aix Marseille University, IUSTI, UMR 7343 CNRS-, F-13453, Marseille, France
Corresponding authors: minhchienxf@gmail.com, olivier.asserin@cea.fr

## ABSTRACT

The fluid flow in weld pool can play a prominent role in the weld quality as well as in the shape of the weld bead seam. It is influenced by several process parameters and operating conditions such as current intensity, welding speed, chemical composition of the material and welding positions. A coupled model that accounts for electromagnetism, heat transfer and fluid flow with moving free surface has been developed. It aims at predicting temperature field, fluid flow velocity in the melting pool and shape of weld joints for various operating parameters. Numerical simulations are carried out with our in-house finite element code Cast3M [1] to study the influence of welding positions: flat, horizontal, vertical up, vertical down and overhead. It turns out that there exists a strong sensitivity of the molten pool shape to welding positions due to different gravity direction. The present work enables us to undertake the development of a more advanced numerical model that will include metal filling.

Keywords: Gas Tungsten Arc Welding (GTAW), welding positions, finite element analysis.

## INTRODUCTION

Gas Tungsten Arc (GTA) welding designates welding processes in which local melting of workpieces to be joined is obtained by the heat flux transferred by an electric arc. They usually produce high quality welds with almost all metals and allows accurate control, thus it is widely used in both mechanized and robotic welding. This welding process is characterized by the simultaneous presence of solid and liquid phases along with plasma arc.

The electric arc and resulting weld pool interact each other very closely in a two-way coupling, so they should be considered all together. In following such an approach, numerical models usually assume axial symmetry in order to reduce computational time [2, 3, 4]. However these models do not accurately predict important quantities such as the size of the weld pool since temperature and velocity do not behave axisymmetrically. Therefore,

to obtain more accurate predictions one has to perform three-dimensional (3D) computations accounting for cathode, arc plasma and anode. So, the development of comprehensive 3D model is complex and requires long computing time. A review of the literature reveals that most authors deal with 3D arc plasma models and weld pool ones, separately. A few 3D weld pool models for GTA welding are available in the literature such as the one of Zhao and al. [4], Zhang and al. [5], Koudadje [6] and Traidia [7]. However in their studies, it is assumed that the surface tension gradient is fixed to an arbitrary constant value [4, 5] or that the surface is not deformable [6], or welding velocity is not accounted for [5].

In order to evaluate the weldability a thorough knowledge of the fluid flow in the weld pool is necessary. Because experimental determination of correct welding procedures for each new application can be very costly and time consuming, computations are welcome in order to understand the physics as well as to optimize the process. Moreover, depending on the assembly configuration welding may need to be performed in another position than flat. This affects the weld pool fluid flow and hence the related weld bead profile. To the best of the authors' knowledge, no study in the open literature presents GTA welding computations in various welding positions. Therefore the objective of this work is to develop a numerical model for GTA welding that is able to predict relevant features of the weld pool in different welding configurations. The present model has been further developed with respect to previous works to account for 3D configurations with deformable free surface. It accounts for electromagnetic field, coupled heat transfer and fluid flow in the assembly and computation of the free surface geometry of the weld pool. In this paper, we have reported and compared the weld pool shapes for various welding positions such as flat (1G), horizontal (2G), vertical up (3G upward), vertical down (3G downward) and overhead (4G), which is the main contribution of this work.

## GOVERNING EQUATIONS

A 3D model accounting for the relevant welding parameters, but reduced to the welding assembly is derived below with the following assumptions. The electric arc is modeled by its heat flux, arc pressure and current applied to the deforming free surface below the welding torch with a Gaussian distribution. We look for a steady state solution by solving the electromagnetic, continuity, momentum and energy equations in the fluid phase, and the electromagnetic and energy equations in the solid phase. The liquid metal is considered as a Newtonian fluid in laminar flow under the Boussinesq's approximation. Moreover, the shape of the weld pool with a deforming free-surface is an outcome of the model. Finally, the velocity of the welding torch is assumed constant and the problem is set in a coordinate system attached to it.

The model accounts for the coupling between electromagnetism, heat transfer and free-surface fluid flow in the weld pool, modeled by Maxwell (eq. 1), Navier-Stokes (eq. 3, 4) and energy conservation equations (eq. 8), respectively. The computational domain used for the 3D weld pool calculations is depicted in figure 1.

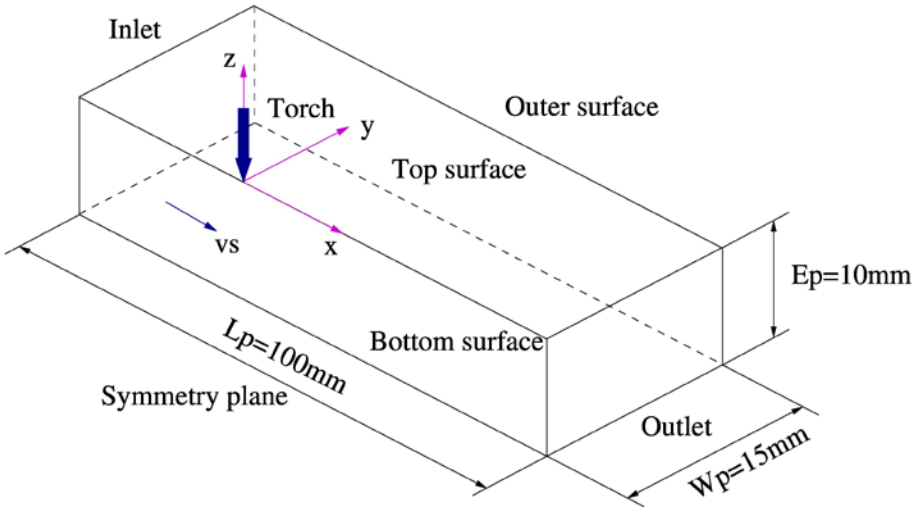


**Fig. 1** Sketch of the 3D computational domain.

## ELECTROMAGNETIC EQUATIONS

The electromagnetic field in the workpiece is computed from the static Maxwell's equations:

$$\nabla \cdot \left( -\sigma \nabla \phi \right) = 0 \tag{1a}$$

$$\nabla \cdot \vec{B} = 0 \tag{1b}$$

$$\nabla \times \vec{B} = \mu_0 \vec{j} \tag{1c}$$

Where $\sigma$ is the electrical conductivity, $\phi$ the scalar electric potential, $\vec{B}$ the magnetic induction, $\mu_0$ the magnetic permeability and $\vec{j} = -\sigma \nabla \phi$ the electric current density.

The electromagnetic boundary conditions are:

$$\vec{B} \cdot \vec{n} = 0 \qquad \textit{on all the surfaces} \tag{2a}$$

$$\nabla \phi \cdot \vec{n} = s_\phi \qquad \textit{on the top surface} \tag{2b}$$

$$-\nabla \phi \cdot \vec{n} = 0 \qquad \textit{on the bottom surface} \tag{2c}$$

$$\phi = 0 \qquad \textit{on the other surfaces} \tag{2d}$$

Where $s_\phi$ is the incoming electric flux and $\vec{n}$ the outward unit normal.

## NAVIER-STOKES EQUATIONS

*Continuity equation:*

$$\nabla \cdot \vec{u} = 0 \tag{3}$$

*Momentum equation:*

$$\rho\left(\vec{\nabla}\vec{u}\right)\cdot\left(\vec{u}-\vec{u}_s\right) = -\nabla p + \vec{\nabla}\cdot\mu\left(\vec{\nabla}\vec{u}+\vec{\nabla}^t\vec{u}\right) + \vec{f}_{\text{Bou}} + \vec{f}_{\text{Lor}} + \vec{f}_{\text{Ext}} \tag{4}$$

Where $\vec{u}$ is the velocity in the melted pool, $\vec{u}_s$ the welding velocity, $\rho$ the density, $p$ the pressure, $\mu$ the dynamic viscosity, with the buoyancy force:

$$\vec{f}_{\text{Bou}} = -\rho_{\text{ref}}\beta(T - T_{\text{ref}})\vec{g} \tag{5}$$

the Lorentz force:

$$\vec{f}_{\text{Lor}} = \vec{j} \times \vec{B} \tag{6}$$

and the velocity extinction force:

$$\vec{f}_{\text{Ext}} = -c(1 - f_l)\vec{u} \tag{7}$$

$\rho_{\text{ref}}$ is a reference density, $\beta$ the thermal expansion coefficient at $T_{\text{ref}}$, a reference temperature. The liquid fraction $f_l$ is assumed to vary linearly with temperature inside the mushy zone [9] and $c$ is a large numerical constant ($c = 10^{12}$).

The fluid flow boundary conditions are:

$$\vec{u} = \vec{0} \qquad \textit{on the solid/liquid interface} \tag{8a}$$

$$\vec{u}\cdot\vec{n} = 0 \qquad \textit{on the top surface and symmetry plane} \tag{8b}$$

$$\vec{u}\cdot\vec{n} = \vec{u}_s\cdot\vec{n} \qquad \textit{on the inlet} \tag{8c}$$

$$\left(\mu\left(\vec{\nabla}\vec{u}+\vec{\nabla}^t\vec{u}\right)\cdot\vec{n}\right)\cdot\vec{t} = \vec{f}_{\text{Mar}}\cdot\vec{t} \qquad \textit{on the top surface} \tag{8d}$$

Where the Marangoni force is:

$$\vec{f}_{\text{Mar}} = \frac{\partial\gamma}{\partial T}\nabla_s T \tag{9}$$

and $\vec{t}$ the tangent vector to the free surface, $\frac{\partial\gamma}{\partial T}$ is the thermal coefficient of surface tension. It depends on temperature and sulfur composition of the steel, modeled by Sahoo's relationship [8].

Different welding positions are computed by setting tilt angles $\alpha_1$ and $\alpha_2$ between gravity and reference frame of the plate (see figure 2). The welding positions considered in this work are: flat (1G), horizontal (2G), vertical up (3G upward), vertical down (3G downward) and overhead (4G). Their corresponding values for the angles $\alpha_1$ and $\alpha_2$ are given in table 1.

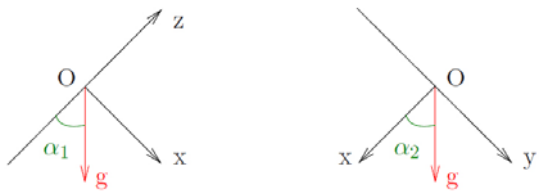


**Fig. 2** Gravity direction in the reference frame defined by angles $\alpha_1$ and $\alpha_2$.

**Table 1.** Angles $\alpha_1$ and $\alpha_2$ related to the welding positions considered in this work.

| Position | 1G | 2G | 3G downward | 3G upward | 4G |
|---|---|---|---|---|---|
| $\alpha_1$ | 0° | 90° | 90° | -90° | 180° |
| $\alpha_2$ | 0° | 90° | 0° | 0° | 0° |

*Free surface equation:*

The total potential energy minimization of the surface leads to the free surface equation:

$$-p+\left(\mu\left(\vec{\nabla}\vec{u}+\vec{\nabla}^{t}\vec{u}\right)\cdot\vec{n}\right)\cdot\vec{n}+\rho g\left(x\sin\alpha_1\cos\alpha_2+y\sin\alpha_1\sin\alpha_2+z\cos\alpha_1\right)=\frac{\gamma(T)}{R(x,y)}+\vec{f}_{Arc}\cdot\vec{n} \tag{10}$$

Where $\gamma$ is the surface tension coefficient, $R(x,y)$ the radius of curvature, $\vec{f}_{\mathrm{Arc}}$ the arc pressure and *x*, *y*, *z* are the free surface coordinates with $z=0$ being the undeformed free surface. We assume that the total volume of the weld pool is kept constant during surface deformation and that the solid part of the workpiece remains undeformed. This leads to the following constraint and boundary conditions:

$$\int_S z(x,y)\,\mathrm{d}x\mathrm{d}y=0 \qquad \textit{on the free surface} \tag{11a}$$

$$z(x,y)=0 \qquad \textit{on the edge of the domain} \tag{11b}$$

## ENERGY EQUATION

The solid/liquid phase change is accounted for with an enthalpy formulation in the energy conservation equation:

$$\rho\left(\vec{\nabla}h\right)\cdot\left(\vec{u}-\vec{u}_s\right)=\vec{\nabla}\cdot\lambda\nabla T+s_{\text{Joule}} \tag{12}$$

Where $h$ is the enthalpy per mass unit, $T$ the temperature, $\lambda$ the thermal conductivity and $s_{\text{Joule}}=\vec{j}\times\vec{E}$ the volumetric heat source from the Joule effect.

The heat transfer boundary conditions are:

$$T=T_0 \qquad \textit{on the inlet} \tag{13a}$$

$$-\lambda\nabla T\cdot\vec{n}=0 \qquad \textit{on the symmetry plane and outlet} \tag{13b}$$

$$\lambda\nabla T\cdot\vec{n}=s_{\text{r}}+s_{\text{c}}+s_{\text{s}} \qquad \textit{on the other surfaces} \tag{13c}$$

With the radiative loss: $s_{\text{r}}=-\varepsilon\sigma_B\left(T^4-T_\infty^4\right)$, the convective heat loss: $s_{\text{c}}=-h_c\left(T-T_\infty\right)$ and $s_{\text{s}}$ the heat source on the surface. $T_\infty$ is the ambient temperature, $\sigma_B$ the Stefan-Boltzmann constant, $h_c$ the convective heat transfer coefficient and $\varepsilon$ the emissivity of the body surface.

## RESULTS AND DISCUSSION

The present computations have been carried out with Cast3M Finite Element code [1] developed at the French Alternative Energies and Atomic Energy Commission (CEA). The results of the model in several welding positions (flat, horizontal, vertical up, vertical down and overhead) are presented to understand the effect of gravity on the weld shape. A box half domain of 150000 elements is considered except in the non-symmetrical 2G case where the full domain is considered. The half domain dimensions are: 100 mm of length, 15 mm of width and 10 mm of depth. The initial temperature is 300 K. The mesh is strongly refined in the weld pool region (14×6×2.5 mm), which is located under the welding torch. In this part of the domain, the minimum element size is 0.18×0.18×0.09 mm. The thermophysical properties of 304L stainless steel are temperature dependent and drawn from Traidia [7], Kim [9] and Sahoo [8]. To compute weld pools of comparable sizes for all the considered welding positions, the following welding parameters have been selected: sulfur content: 0.001 wt%, welding speed: 20 cm.min$^{-1}$, arc pressure: 100 Nm$^{-2}$, electric current: 150 A, voltage: 10 V and process efficiency of 0.68. Relevant computed quantities are reported in table 2.

**Table 2.** Computed quantities for various welding positions.

| Case | $T_{max}$ (K) | $u_{max}$ (m $s^{-1}$) | Length (mm) | Width (mm) | Depth (mm) |
|---|---|---|---|---|---|
| 1G | 2425 | 0.21 | 7.34 | 3.12 | 0.83 |
| 2G (full mesh) | 2421 | 0.19 | 8.54 | 3.60 \| 3.05 | 0.92 |
| 3G upward | 2308 | 0.25 | 7.65 | 3.01 | 1.27 |
| 3G downward | 2385 | 0.19 | 7.12 | 3.36 | 1.06 |
| 4G | 2398 | 0.20 | 7.44 | 3.13 | 0.96 |

Figures 3, 4, 5 and 6 present the temperature field and the weld pool shapes for flat, overhead, vertical up, vertical down and horizontal configurations, respectively. Simulation results show that the welding position influences significantly the shape of the weld particularly that of the surface. Although not shown here, we mention that the flows in the weld pool for the various welding positions are quite similar.

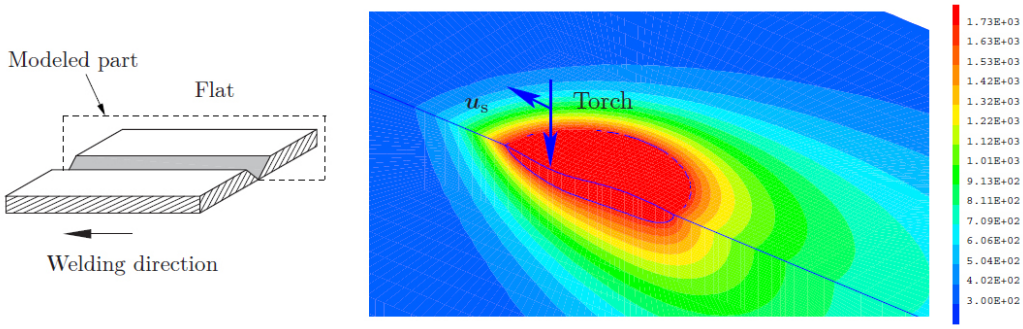


**Fig. 3** Temperature field (K) and weld pool limit for the flat case (1G).

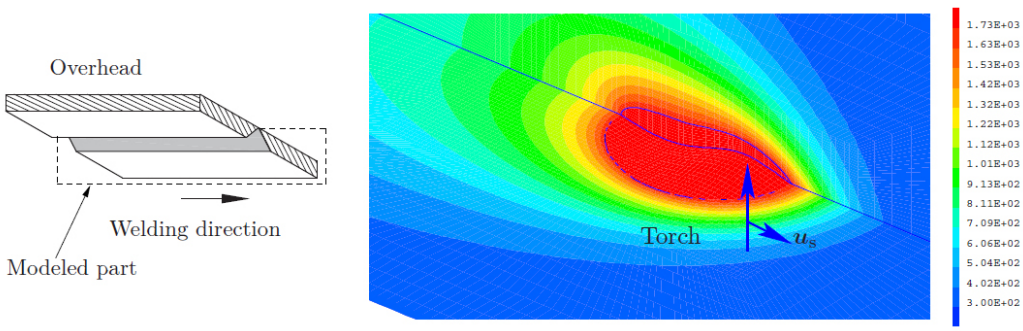


**Fig. 4** Temperature field (K) and weld pool limit for the overhead case (4G).

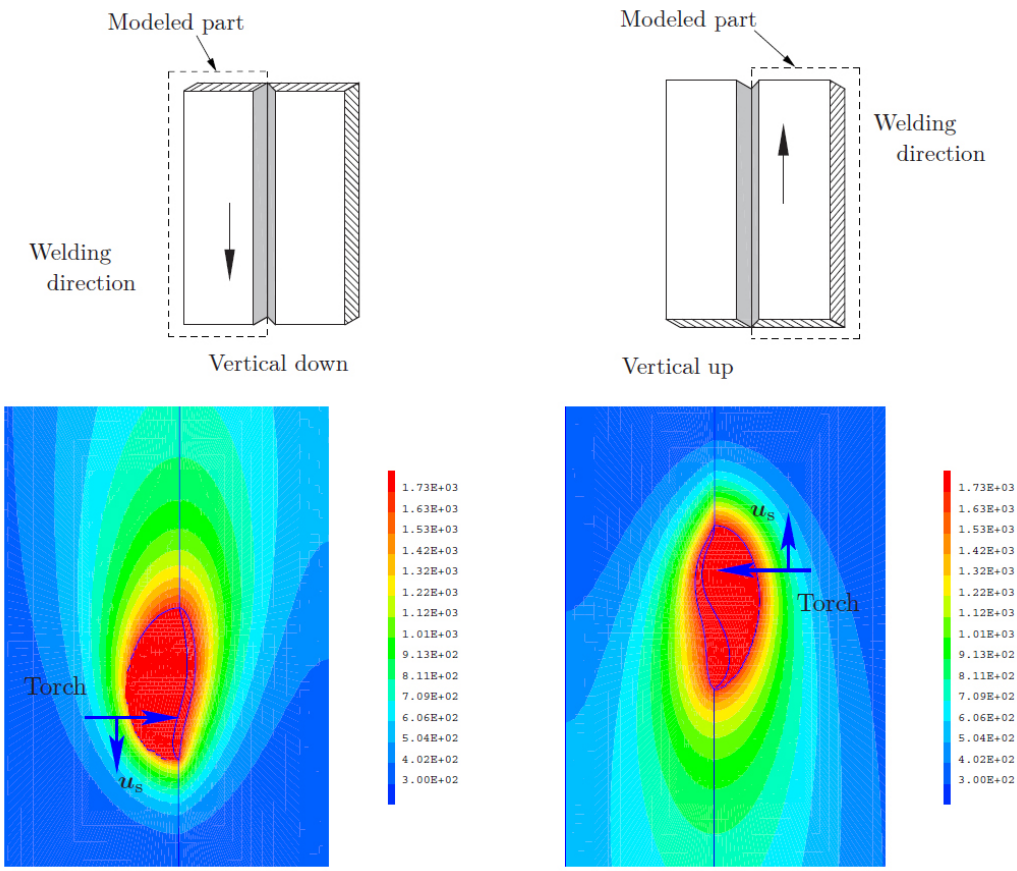


**Fig. 5** Temperature field (K) and weld pool limit for the vertical down (3G downward) and vertical up (3G upward) cases.

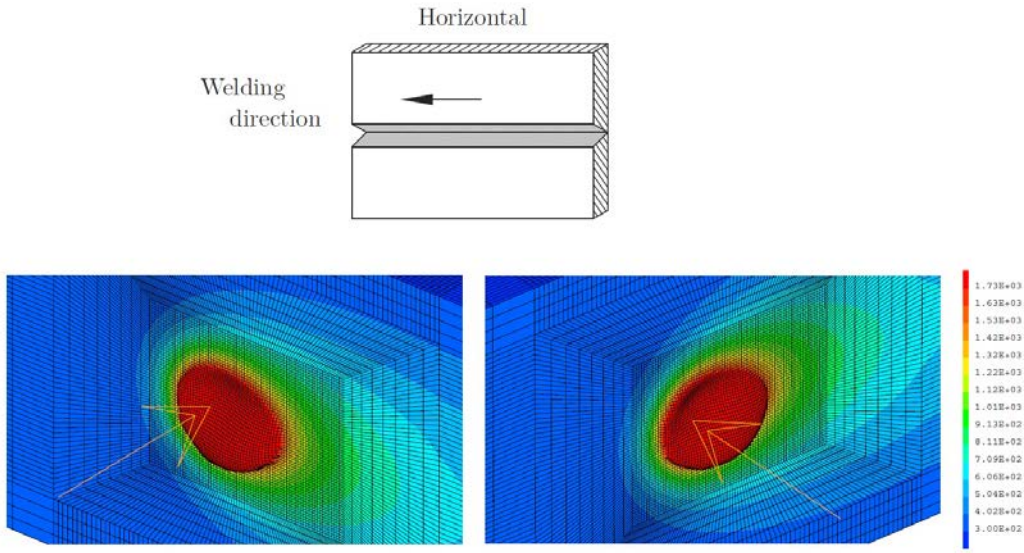


**Fig. 6** Temperature field (K) in the weld pool for the horizontal position (2G), view from right to left (left) and view from left to right (right).

As expected, the weld pool free surface deforms according to the gravity direction (3G downward case, 3G upward case and 2G case), which tends to draw the molten pool free surface in this direction (figures 5, 6). Indeed, gravity pulls the liquid metal from upper towards lower melted pool regions. It can be observed from table 2 and figures 3, 4 that the weld bead shape are quite similar in cases 1G and 4G. Indeed, as gravity is perpendicular to the welding plane, the liquid metal on the free surface does not flow in this plane. However, in the overhead welding position (4G) a necessary condition for weldability is that surface tension force remains sufficiently large to counteract the gravity force. For horizontal position 2G, the weld bead deformation is clearly asymmetrical about the longitudinal median plane. The calculated widths of the bottom part and the upper part are 3.60 mm and 3.05 mm respectively. Because the gravity pulls the free surface down, the liquid metal is moved downward in the direction of gravity, which causes the swelling of the weld in the bottom part, increases the weld depth in the upper part (figure 6) and finally inducing asymmetry in the shape of the weld bead seam. Furthermore, in the vertical up welding position (3G upward), a maximum depth of 1.27 mm is obtained, which is greater than that in the other welding positions (table 2). Indeed, the gravity transports mass downward and away from the arc, exposing the underlying material and causing more penetration. A similar trend was observed in Kumar [10] for gas metal arc welding (GMAW).

## CONCLUSIONS

In this paper, a model of heat transfer and fluid flow for the GTA welding has been developed, that is capable of simulating the temperature and velocity fields, predict the weld pool shape and understand the effects of welding positions on the free surface profile.
The model solves for the electromagnetic, continuity, momentum and energy equations taking into account free surface deformations and phase change. A steady solution for the temperature, velocity field and free surface of the weld pool has been found. This model is able to simulate the main welding positions that significantly affect the free surface profile but they do not change the flow pattern in the weld pool. The free surface of the weld pool deforms according to the gravity direction (2G, 3G upward and 3G downward cases). In the 2G case, the width of the weld bead is asymmetric about the electrode position. Finally, the shape of the weld pool in the two cases 1G and 4G are quite similar. Experimental verification of computations in various welding positions and accounting for metal filling will be considered in a future work.

## REFERENCES


[1] CAST3M SOFTWARE: *CEA Saclay*, Downloadable at: http://www-cast3m.cea.fr/, 2015.

[2] M. TANAKA, H. TERASAKI, M. USHIO and J. J. LOWKE: 'A unified numerical modeling of stationary tungsten inert gas welding process', *Metallurgical and materials transactions A*, 33(7):2043–2052, 2002.

[3] H. G. FAN and R. KOVACEVIC: 'A unified model of transport phenomena in gas metal arc welding including electrode, arc plasma and molten pool', *Journal of Physics D: Applied Physics*, 37(18):2531–2544, 2004.

[4] P. C. ZHAO, C. S. WU and Y. M. ZHANG: 'Modelling the transient behaviours of a fully penetrated gas-tungsten arc weld pool with surface deformation', *Proceedings of the Institution of Mechanical Engineers, Part B: Journal of Engineering Manufacture*, 219(1):99–110, 2005.

[5] W. ZHANG, G. G. ROY, J. W. ELMER and T. DEBROY: 'Modeling of heat transfer and fluid flow during gas tungsten arc spot welding of low carbon steel', *Journal of Applied Physics*, 93(5):3022–3033, 2003.

[6] K. KOUDADJE: *Étude expérimentale et modélisation numérique du bain de fusion en soudage TIG d'aciers (Experimental and numerical modeling of GTA weld pools of steels)*, PhD thesis, Université Aix-Marseille - EDF, 2013.

[7] A. TRAIDIA: *Multiphysics modelling and numerical simulation of GTA weld pools*, PhD thesis, École Polytechnique, 2011.

[8] P. SAHOO, T. DEBROY and M. J. MCNALLAN: 'Surface tension of binary metal-surface active solute systems under conditions relevant to welding metallurgy', *Metallurgical transactions B*, 19(3):483–491, 1988.

[9] C. S. KIM: 'Thermophysical properties of stainless steels', Technical report, Argonne National Lab., 1975.

[10] A. KUMAR and T. DEBROY: 'Heat transfer and fluid flow during gas metal arc fillet welding for various joint configurations and welding positions', *Metallurgical and materials transactions A*, 38(3):506–519, 2007.